Journal of Science and Technology in Civil Engineering, HUCE (NUCE), 2022, 16 (3): 97–110

ASSESSING THE SHEAR BEHAVIOR OF STEEL FIBER REINFORCED CONCRETE BEAMS CORRODED UNDER CHLORIDE ATTACKS

Nguyen Thi Thanh Thao[a], Tran Phi Son Tung[a], Nguyen Duc Nhan[a], Nguyen Ngoc Tan[a,*]

[a]*Faculty of Building and Industrial Construction, Hanoi University of Civil Engineering, 55 Giai Phong road, Hai Ba Trung district, Hanoi, Vietnam*

Article history:
Received 12/4/2022, Revised 10/5/2022, Accepted 18/5/2022

Abstract

Steel corrosion affects the failure mechanism of deteriorated reinforced concrete (RC) beams. Meanwhile, there is a lack of research on the shear behavior of corroded RC beams, particularly corroded steel fiber reinforced concrete (SFRC) beams. This paper investigates the shear behavior of corroded SFRC beams with a 1.5 shear span-to-depth ratio. All beam specimens included steel fibers with 50 kg/m^3. In particular, tensile longitudinal reinforcements were subjected to a corrosion degree of 16.4%, while stirrups were subjected to an approximately 24.1% corrosion degree. These results are compared to those obtained on a non-corroded beam. The obtained results from the four-point loading tests show that the corroded SFRC beams preserve a softening behavior as opposed to the sudden shear failure of RC beams without steel fibers.

Keywords: shear behavior; steel fiber reinforced concrete; reinforced concrete beam; steel corrosion.

https://doi.org/10.31814/stce.huce(nuce)2022-16(3)-08

1. Introduction

Nowadays, there are undoubtedly several benefits of steel fiber reinforced concrete (SFRC). One of the primary positives of SFRC is that it improves the mechanical properties of traditional concrete, particularly the tensile strength [1, 2]. This means that the bridging actions of steel fibers on cracks in SFRC during loading could help to reduce crack width. Moreover, one of the advantages of SFRC is crack resistance in enhanced post-crack strength.

The addition of steel fibers to concrete that may be used to enhance the mechanical properties has been studied experimentally. Nguyen et al. [3] found the following results after testing sample groups constructed of SFRC with varying steel fiber contents: (i) When the steel fiber content was raised, the tensile strength of SFRC grew from 8 to 97%; (ii) Unlike traditional concrete, the addition of steel fibers enhanced the ductility response. Likewise, another research work conducted by Bui et al. [4] presented that when added steel fibers splitting tensile strength and flexural tensile strength significantly increased by up to 228% and 145%, respectively. Steel fiber addition to beam structures exhibited more ductility than ordinary concrete in the post-peak stage.

On the other hand, shear failure is a critical issue in the RC beams because of the brittle behavior [5]. Shear strength is generally predicted using the geometric theory of the shear resistant mechanism.

*Corresponding author. *E-mail address:* tannn@huce.edu.vn (Tan, N. N.)

According to the design code ACI 318-19 [6], if a ratio of shear span-to-effective depth (a/d) is less than 2, beams are classified as deep beams with an arch action for the shear resistant mechanism. However, a beam action mechanism is a way of load transfer in shear for beams having an a/d ratio of greater than 2.0. Meanwhile, current building constructions in Vietnam have been frequently subjected to harsh environmental conditions, which exacerbate the corrosion of RC structures. Steel corrosion is a severe problem that occurs in the loss of bond between concrete and steel reinforcement resulting in a decrease in both flexural and shear capacity of RC structures [7–9]. Soltani et al. [7] reported that flexural and shear strengths of beam specimens were reduced to 80% in corrosive environments. Besides, previous studies have shown that the failure modes of corroded RC structures can change into brittle failure due to a higher degree of corrosion, especially in shear performance [10–14]. It was shown in the study of Nguyen et al. [15] that steel corrosion may modify the shear transferring mechanism of corroded RC beams. For example, beam specimens with an a/d ratio less than 2.0 might have the load transferring mode changing from the combination of beam action and arch action to mainly arch action. However, beams with an a/d ratio greater than 2.0 may fail in diagonal tension failure by beam action.

Numerous researches have investigated the influence of steel fibers on the ability of concrete structures in flexural and shear capacity based on the improved ductile performance in SFRC [16–21]. Particularly, Bui et al. [4] further claimed that steel fibers with a high-volume fraction of greater than 1.2% were capable of replacing stirrups to ensure shear capacity because of the similar behavior to traditional RC beams. Additionally, Kwak et al. [19] investigated that beams with an a/d ratio of 2.0 failed in a combination of shear and flexure, whereas beams with a higher a/d ratio only failed by flexure. However, Biolzi et al. [21] argued that beams with an a/d ratio of 1.5 still failed by arch action with a ductile post-peak part.

The steel fibers in concrete not only improve the overall flexural and shear resistance but also is an effective method for corrosion resistance. Furthermore, steel fibers could restrain the propagation of corrosion-induced cracks due to the restricted migration and diffusion transport capabilities of concrete [22, 23]. Taqi et al. [24] carried out experimental works that discussed the influence of corrosion on the shear behavior of SFRC beams having a 2.8 a/d ratio with or without pre-corroded steel fiber. They claimed that increasing the steel fiber content causes the failure mode to change from shear to flexural failure.

Apart from the advantages of steel fibers on concrete properties and structural behavior, the corrosion resistance of SFRC is rarely considered. The present experiment in this paper focuses on the shear performance of one control and two corroded SFRC beams with a 0.6% volume fraction of steel fiber hooked-end type (corresponding to 50 kg/m^3). First, the corroded beam specimens were taken to an accelerated corrosion test with 16.4% and 24.1% average degrees of corrosion for tensile longitudinal reinforcement and stirrups. Then, after determining the material properties, three beam specimens constructed entirely of steel fiber reinforced concrete were subjected to a four-point loading test. Finally, the findings on the role of steel fibers in the shear behavior of SFRC beams by chloride attacks through the experimental study were discussed.

2. Experimental program

2.1. Materials

Table 1 shows the designed mixture of SFRC used. As with ordinary concrete, Portland cement PCB40 was used as the binder, while river sand and crushed stone were used for fine and coarse

aggregates. The steel fibers with a content of 50 kg/m^3 by mass were used in the SFRC 50 mix. These steel fibers are manufactured from stainless steel provided by Bekaert. The experimental works used Dramix 3D 65/35BG steel fibers deformed in 3D with hooked ends to increase anchoring in the concrete matrix, as shown in Fig. 1. In particular, the elastic modulus of the fiber was around 210 GPa, and the tensile strength was 1345 MPa. The aspect ratio of fiber length to diameter (l_f/d_f) was 65 for defining the properties of the fibers (corresponding to a length l_f of 35 mm and a diameter d_f of 0.55 mm).

Figure 1. Dramix 3D 65/35BG hooked-end steel fibers

Table 1. Concrete mix

Mix	Cement (kg/m^3)	Fine aggregates (kg/m^3)	Coarse aggregates (kg/m^3)	Water (liter/m^3)	Ratio W/C	Steel fiber (kg/m^3)
SFRC 50	477	596	1250	185	0.39	50

The cubes with the dimensions of 150×150×150 mm were cast, cured in indoor environmental conditions of the laboratory, and tested to determine compressive strength. As a result, the mean compressive strength of a set of three SFRC cubes at 28 days was 49.8 MPa, as shown in Table 2, equivalent to the concrete C40/50, as defined in Eurocode 2 (EC2) [25].

Table 2. Compressive strength of SFRC specimens

Sample	Maximum compressive load (kN)	Compressive strength (MPa)	Mean compressive strength (MPa)	Standard deviation (MPa)	Coefficient of variation (%)
M1	1102.0	49.0			
M2	1112.7	49.5	49.8	1.0	2.0
M3	1145.2	50.9			

In this study, beam specimens used longitudinal reinforcements of 10-mm and 12-mm diameter and stirrups of 6-mm diameter, as illustrated in Fig 2. There are three sets of steel rebars and each of which has three specimens manufactured from the same strength grades of steel. The yield and ultimate tensile strengths of steel reinforcements were determined by the tension test. The obtained results are synthesized in Table 3.

2.2. SFRC beam specimens

According to the SFRC mixture, three beam specimens were conducted. The first beam, named B1.1-NC, is the non-corroded SFRC beam as the control beam, while two beams, denoted B2.1-C

Table 3. Tensile strength of steel reinforcements

Sample	Diameter/ steel type	Yield tensile load (kN)	Ultimate tensile load (kN)	Yield tensile strength (MPa)	Mean yield tensile strength (MPa)	Ultimate tensile strength (MPa)	Mean ultimate tensile strength (MPa)
M1	ϕ12 mm CB300-V	41.5	60.5	366.9	374.3	534.9	543.2
M2		43.0	62.5	380.2		552.6	
M3		42.5	61.3	375.8		542.0	
M1	ϕ10 mm CB300-V	28.9	44.2	368.3	366.9	563.2	565.4
M2		28.5	44.5	363.1		566.9	
M3		29.0	44.4	369.4		566.0	
M1	ϕ6 mm CB240-T	9.5	14.7	335.5	331.1	519.1	514.8
M2		9.1	14.5	321.6		512.4	
M3		9.5	14.5	336.3		513.0	

and B3.1-C, are subjected to the accelerated corrosion test. Fig. 2 illustrates the dimension and layout of the beam specimens. In more detail, the beam specimens have a width of 150 mm, a height of 200 mm, and a length of 1100 mm. Three beams were reinforced with two ϕ10 mm and two ϕ12 mm steel rebars in the top and bottom layers, respectively. Additionally, all beam specimens were installed with ϕ6 mm stirrups with a regular spacing of 150 mm. The concrete cover is 40 mm in thickness according to the Vietnamese standard TCVN 9346:2012 [26] for RC structures in aggressive conditions.

2.3. Accelerated electrochemical corrosion test

Analyzing the load-carrying capacity of corroded RC beams under normal service conditions is more challenging, depending on the corrosion rate [27]. In this study, an accelerated electrochemical corrosion test was conducted to produce experimental specimens that exhibit the same corrosion behavior as in reality in a shorter period. Two beam specimens were immersed in a 3.5% sodium solution (NaCl) for 48 hours for concrete total saturation. The accelerated electrochemical corrosion test on the beam specimens is shown in Fig. 3. Simultaneously, chloride ions diffused into the corrosion test specimens from the electrolyte solution. Each transformer was connected to the longitudinal rebars at the bottom layer of corroded beams. Each longitudinal rebar received an electrical current of 1A maintained constant during the corrosion test process. Finally, corrosion testing of SFRC beams would be completed after 576 hours continuously, which was estimated based on Faraday's law [28].

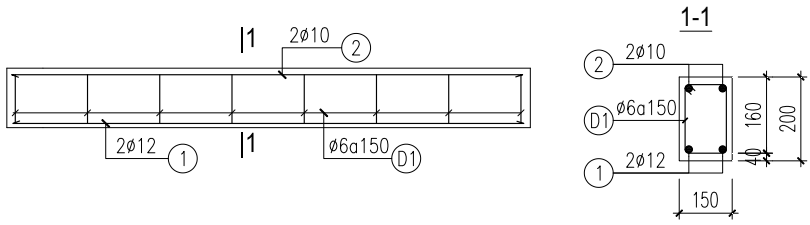

Figure 2. Detailed layout of beam specimens

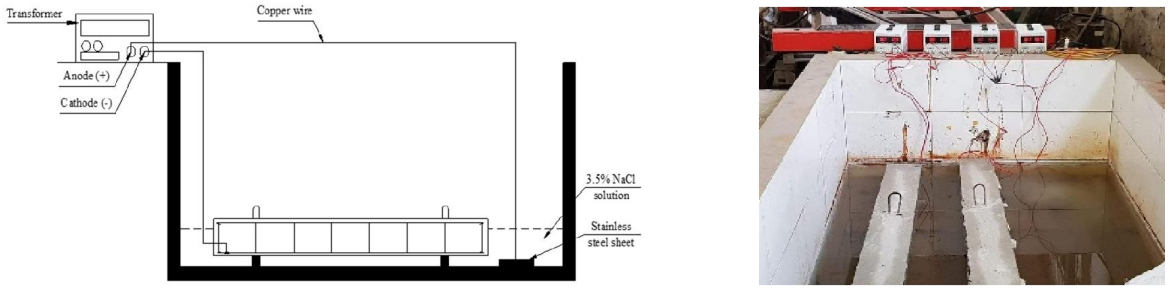

(a) Testing diagram (b) SFRC beams in the solution

Figure 3. Accelerated corrosion test for corroded SFRC beams

2.4. Four-point loading test

Following the corrosion test, an experimental program was carried out on three beam specimens to assess the mechanical behavior of non-corroded and corroded SFRC beams based on several parameters, such as the load-displacement curves, the relationship between load and crack width, cracking pattern, and failure mechanism.

(a) Control beam (b) Corroded beam

Figure 4. Experimental set-up for (a) the non-corroded beam, (b) the corroded beam

Figs. 4 and 5 depict an experimental program of three beams on a four-point loading test. The span of beams between the supports was 900 mm. The load was distributed on beams in two loading application points by a hydraulic jack at a controlled speed. The distance between the two loading points is 450 mm, and the distance between the support and the loading point is 225 mm. So, the shear span-to-depth ratio (a/d) of experimental beams is 1.5. Six linear variable differential transformers (LVDT) were arranged to measure vertical displacements and crack width. For the vertical displacement, devices I_1 and I_3 were placed at the position of two supports, device I_2 was located on the bottom face and at the middle span, and device I_{TH} was located at the beam's neutral axis. For the crack mouth opening displacement (CMOD) of shear cracks, two devices denoted CR_1 and CR_2 were perpendicularly located on the diagonal lines between loading point centers and supports, and a 2-cm distance for the bottom face. All testing devices were connected to a data logger TDS-530 and a laptop computer to automatically record the data.

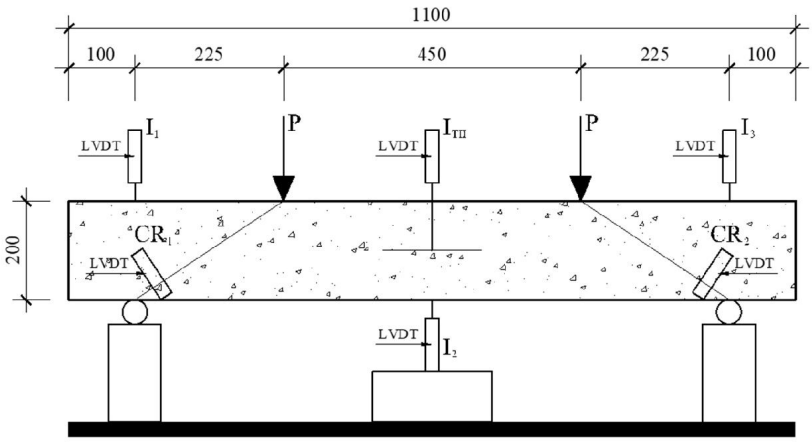

Figure 5. Four-point loading test configuration

3. Experimental results

This study focuses on the shear behavior of non-corroded and corroded SFRC beams. Therefore, four-point loading tests were conducted on all specimens until failure after two beams (B2.1-C and B3.1-C) were subjected to the corrosion process. The results of the accelerated corrosion process and the four-point loading tests are included in this section.

3.1. Actual corrosion degree

In this study, the corrosion degree of each steel reinforcement, denoted c (%), is determined by Eq. (1). Then, the average degree of corrosion, denoted c_m (%), is calculated for all steel reinforcements of the same type.

$$c\,(\%) = \frac{m_o - m}{m_o} = \frac{\Delta m}{m_o} \tag{1}$$

where: m_o (in g) is the original weight of the steel rebar before corrosion, which was measured before casting the beam specimens; m (in g) is the final weight of the rebar after corrosion, which was measured after cleaning; Δm is the mass loss of the steel rebar.

After completing the four-point loading test, all longitudinal reinforcements and stirrups were removed to determine the mass loss of corroded rebars. When the surrounding concrete part of the corroded beams was entirely demolished, corroded rebars were extracted carefully. After an accelerated electrochemical corrosion process, longitudinal rebars and stirrups exhibited corrosion attack, but the stainless steel fibers were maintained corrosion-free, as shown in Fig. 6. In the following step, longitudinal rebars and stirrups were cleaned using HCl solution according to ASTM G1-03 [29]. The residual weights of longitudinal rebars and stirrups were measured, and their corrosion degrees are reported in Table 4. Four longitudinal rebars in each beam specimen are numbered from 1 to 4 with the designation R, while eight stirrups are denoted with the designation S and numbers ranging from 1 to 8. As a result of mass loss, the corrosion degrees of tensile longitudinal rebars and stirrups were 16.4% and 24.1% on average, respectively. Meanwhile, the corrosion degree of compressive longitudinal rebars at the top layer of the beam specimens have small corrosion degrees ranging from 5.4% to 7.0% on average. In this study, the corrosion degree of corroded SFRC beams is considered equivalent to that of tension longitudinal reinforcement at the bottom layer.

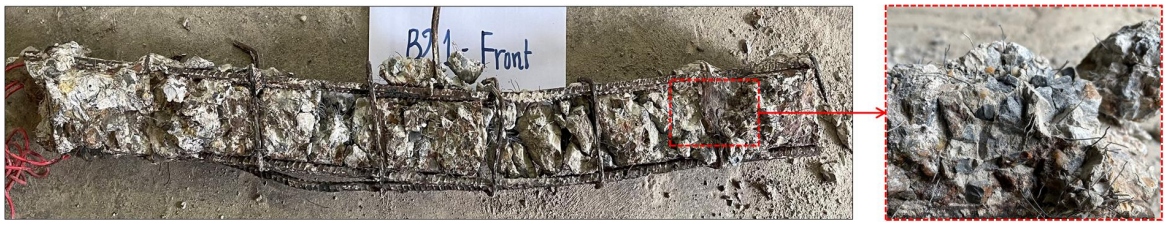

Figure 6. Stage of a corroded SFRC beam when extracting rebars

Table 4. Corrosion results in longitudinal reinforcements and stirrups

Beam	Steel sample	m_o (g)	m (g)	Δm (g)	c (%)	c_m (%)
B2.1-C	R2-1	894.7	744.5	150.2	16.8	16.5
	R2-2	905.5	758.5	147.0	16.2	
	R2-3	625.1	587.5	37.6	6.0	7.0
	R2-4	619.9	570.1	49.7	8.0	
	S2-1	91.7	65.5	26.2	28.6	25.8
	S2-2	91.7	68.0	23.7	25.8	
	S2-3	91.7	68.5	23.2	25.3	
	S2-4	91.7	67.0	24.7	26.9	
	S2-5	100.4	78.5	21.9	21.8	
	S2-6	91.7	67.5	24.2	26.4	
	S2-7	91.7	68.0	23.7	25.8	
	S2-8	91.7	68.8	22.9	25.0	
B3.1-C	R3-1	894.6	774.0	120.6	13.5	16.3
	R3-2	899.1	726.5	172.6	19.2	
	R3-3	626.9	587.8	39.0	6.2	5.4
	R3-4	624.4	595.5	29.0	4.6	
	S3-1	91.7	72.0	19.7	21.5	22.5
	S3-2	101.5	81.5	20.0	19.7	
	S3-3	91.7	72.5	19.2	20.9	
	S3-4	91.7	71.5	20.2	22.0	
	S3-5	91.7	65.0	26.7	29.1	
	S3-6	91.7	69.5	22.2	24.2	
	S3-7	91.7	73.5	18.2	19.8	
	S3-8	91.7	71.5	20.2	22.0	

3.2. Mechanical behavior of the control SFRC beam

The mechanical behavior of the control beam B1.1-NC is analyzed based on the load-displacement curves, as shown in Fig. 7. The solid line shows the mid-span displacement measured at the bottom face (denoted f_b), while the dotted line presents the mid-span displacement measured at the tested beam's neutral axis (denoted f_n). These load-displacement curves could be divided into three main

stages. At first, the stage OA represents the linear behavior of the SFRC beam until the first flexural crack appears. After the cracking load of approximately 80 kN, this beam begins to behave non-linear in stage AB due to the formation of flexural cracks between two loading points, followed by shear cracks from the support to the loading point. In the next stage BC, the vertical displacement continues to increase quickly due to the opening of flexural cracks and shear cracks while maintaining the applied load with a small variation. The control beam reaches the maximum load (denoted $P_{\max}^{NC}$) of 335.87 kN and the corresponding displacement measured at the neutral axis (denoted f_n^{NC}) of 5.88 mm. Then, the concrete in the compression zone is crushed while the tensile longitudinal rebars are yielding. Besides, the shear crack CR_2 is significantly opened on one side of the beam, as shown in Fig. 8. At point C, the displacement f_n is 18.68 mm, corresponding to 1/50 of the span, and the tested beam is considered to have failed by flexural-shear mode. This displacement is greater than the critical value based on current design codes [6, 25]. Therefore, the SFRC beam exhibits a higher ductility behavior instead of the sudden shear failure of traditional RC beams.

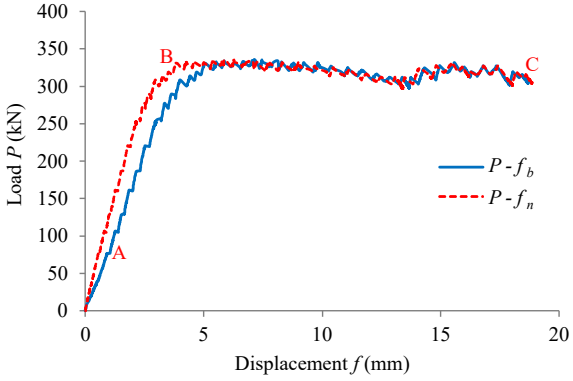

Figure 7. Load-displacement curves of the control beam B1.1-NC

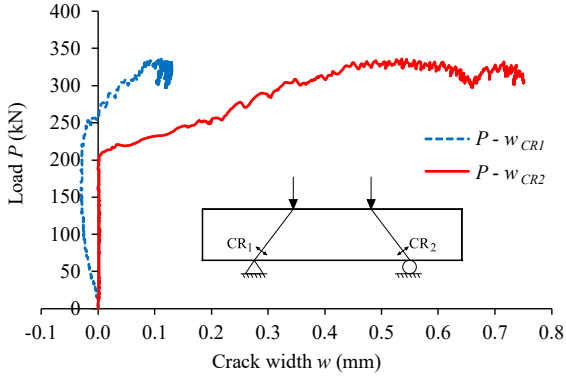

Figure 8. Load-CMOD curves of the control beam B1.1-NC

In this study, the CMOD values of two shear cracks, CR_1 and CR_2, were measured using two displacement devices, as illustrated in Fig. 5. The load-CMOD curves in Fig. 8 show that two shear cracks do not occur under loading with the load less than 200 kN while appearing several flexural cracks. After that, shear crack CR_2 begins to propagate diagonally from the support towards the

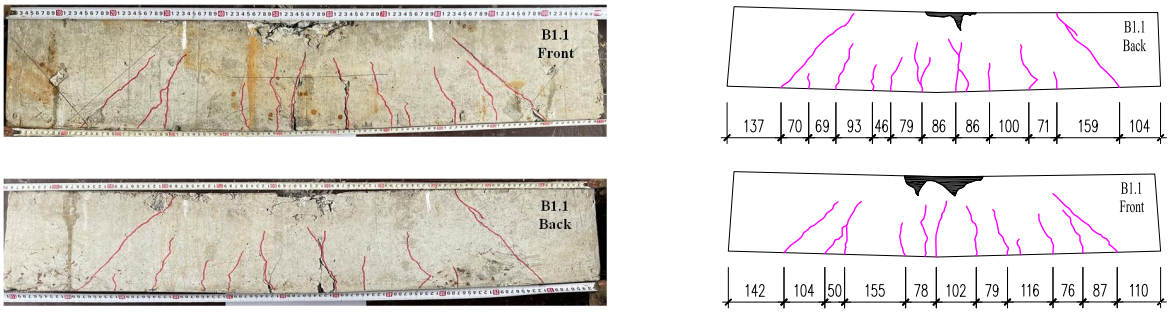

(a) Beam captured at the final state

(b) Cracking pattern

Figure 9. Failure mode and cracking pattern of the control beam B1.1-NC

loading point, while shear crack CR_1 can be observed at the load of 250 kN. As the beam reaches the maximum load, the width (denoted w) of the shear crack CR_1 grows to around 0.1 mm, while the shear crack CR_2 quickly expands to almost 0.5 mm in width, which is over to acceptable crack width according to EC 2 [25]. At the end of the test, the shear crack CR_2 propagated to the compression zone and opened with a 0.8 mm width. The cracking pattern due to loading was captured for the front and back sides of the control beam and presented in Fig. 9.

3.3. Mechanical behavior of the corroded SFRC beams

Similar to the control beam, the mechanical behavior of corroded SFRC beams B2.1-C and B3.1-C is also evaluated based on the curves of load-displacement and load-CMOD, as shown in Figs. 10–13. The load-displacement curves demonstrate that the performance of these corroded beams has deteriorated under the effect of steel reinforcement corrosion, but the mechanical behavior in stages from OA to BC is quite equivalent compared to the control beam. At first, the corroded beams in stage OA operate a quasi-linear behavior since they had several corrosion-induced cracks. At point A, the first flexural crack occurred at the load values of 130 and 135 kN for beams B2.1-C and B3.1-C, respectively. Then, these beams begin to increase the vertical displacement in stage AB, which is described by reducing the slope of the load-displacement curves.

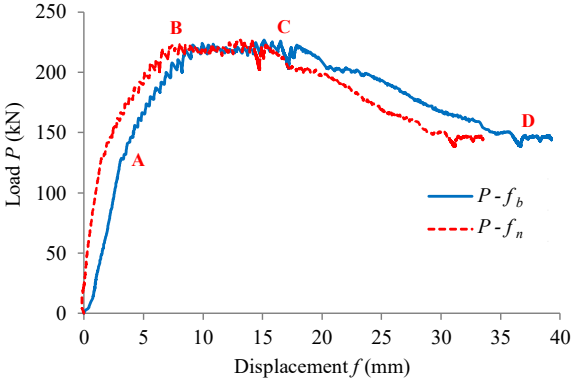

Figure 10. Load-displacement curves of the corroded beam B2.1-C

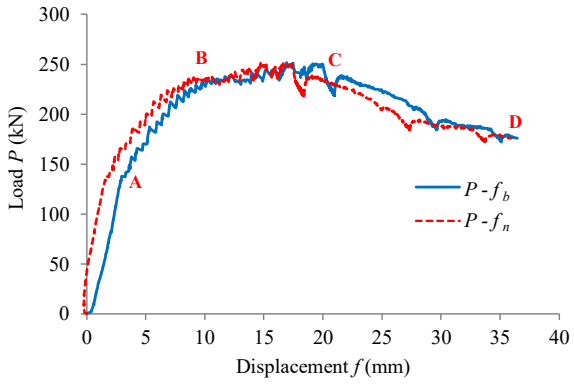

Figure 11. Load-displacement curves of the corroded beam B3.1-C

In the next stage BC, the behavior of the two corroded beams is referred to in the sustaining stage as the control beam. The results show that beam B2.1-C has the maximum load (denoted $P^C_{\max}$) of 226.58 kN at the corresponding displacement measured at the neutral axis (denoted f^C_n) of 13.18 mm (Fig. 10). Meanwhile, the obtained results of beam B3.1-C are $P^C_{\max}$ of 251.90 kN and f^C_n of 14.75 mm, as shown in Fig. 11. Therefore, the average maximum load of these corroded beams equals 239.24 kN. On the other hand, when the applied load reaches 60% of the maximum load, the shear crack CR_1 does not expand, while the shear crack CR_2 begins to open continuously, as can be seen in Figs. 12 and 13. In stage BC, the shear crack CR_2 grows beyond 5 mm. After that, the measured width may be inaccurate due to the separation of the concrete cover near the support.

In the stage CD, the corroded beams were fractured due to the loss of load-carrying capacity. On the corroded beam B2.1-C, the shear crack CR_1 propagates and intersects with the longitudinal crack due to corrosion to become a web-shear crack, as shown in Fig. 14. Besides, the shear crack CR_2 continues to open with a significant width. Due to the ductility of SFRC, both corroded beams have relatively similar cracking patterns until failure. In particular, during the experiment, beam B3.1-C

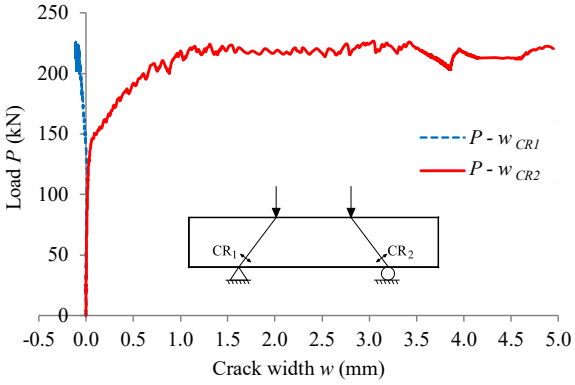

Figure 12. Load-CMOD curves of the corroded beam B2.1-C

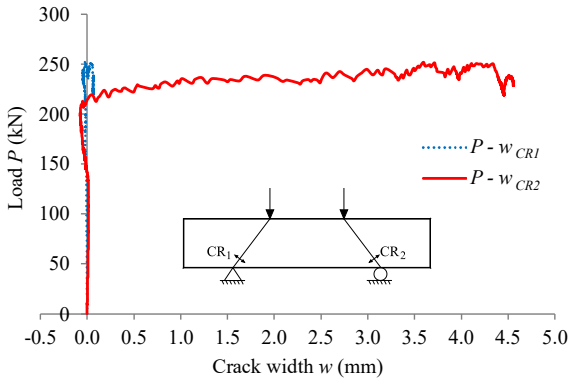

Figure 13. Load-CMOD curves of the corroded beam B3.1-C

suddenly failed at the load of 200 kN owing to the corroded rebar rupture, as shown in Fig. 15. After demolition of surrounding concrete, ruptured steel rebar at the tension layer, named R3-2, was measured to obtain a severe corrosion degree of 19.2%, the highest value among all longitudinal steel rebars, as indicated in Table 4. Therefore, the final failure of this beam is different compared to the tested others.

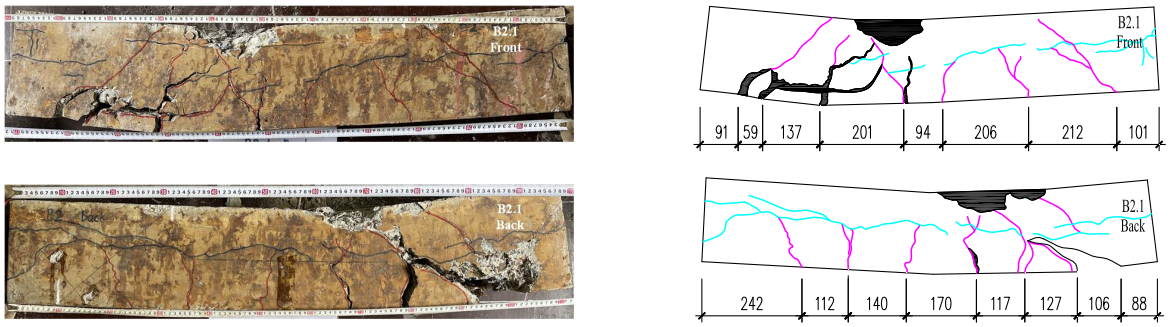

(a) Beam captured at the final state

(b) Cracking pattern

Figure 14. Failure mode and cracking pattern of the corroded beam B2.1-C

Additionally, Figs. 14 and 15 illustrate the failure mode and cracking patterns on two corroded beams. Compared to the control beam, the corroded beams have two types of cracks, including corrosion-induced cracks and cracks due to loading. In the beginning, the corrosion-induced cracks were horizontally distributed along the length of the beam specimens. After conducting the loading test, the flexural cracks began to appear from the bottom of the beam. These cracks tend to develop and intersect with the corrosion-induced cracks as the load increases. The failure is initiated by crushing the concrete in the compression zone, while a flexural crack at the middle span in the tension zone is opened with a significant width. Besides, the shear cracks intersected with the horizontal cracks due to corrosion and propagated quickly to the loading point or crushed concrete zone. The failure mode of the corroded beam B2.1-C is shear-tension, which is characterized by the web-shear cracks that occurred due to the bond loss between corroded longitudinal reinforcement and concrete. Meanwhile, the corroded beam B3.1-C failed by the shear-tension with the corroded rebar rupture.

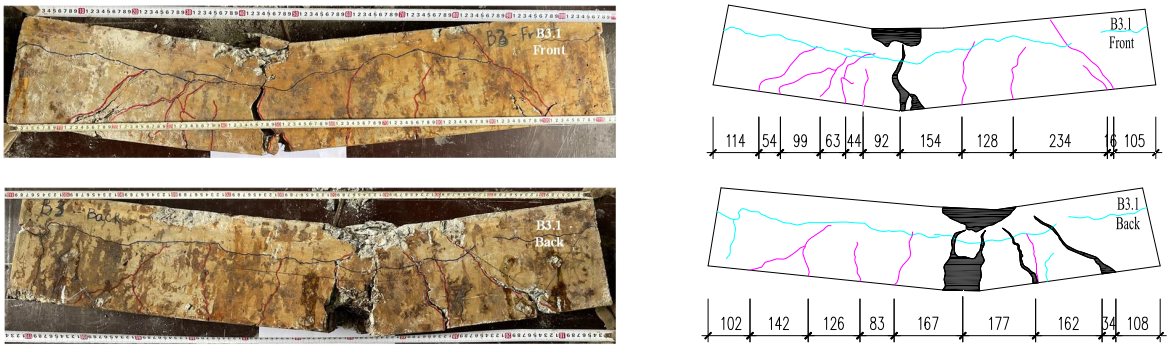

(a) Beam captured at the final state (b) Cracking pattern

Figure 15. Failure mode and cracking pattern of the corroded beam B3.1-C

3.4. Comparisons between control beam and corroded beam

As shown in Fig. 16, the corroded beams have a stiffness smaller than the control beam caused by corrosion damage in the first stages (OA and AB) of loading. In order to compare the load-carrying capacity of three beams, Table 5 shows the specific values of load and displacement for non-corroded and corroded SFRC beams. The maximum loads applied to corroded beams range between 67–75% of that to the control beam. The displacement measured at the corroded beam's neutral axis is 2.24–2.51 times higher than that of the control beam, as indicated in Table 5. Besides, the residual loads of corroded beams were reported as around 43–52% of the maximum load of the control beam. However, the corroded SFRC beams still reflect a ductile behavior in the serviceability state.

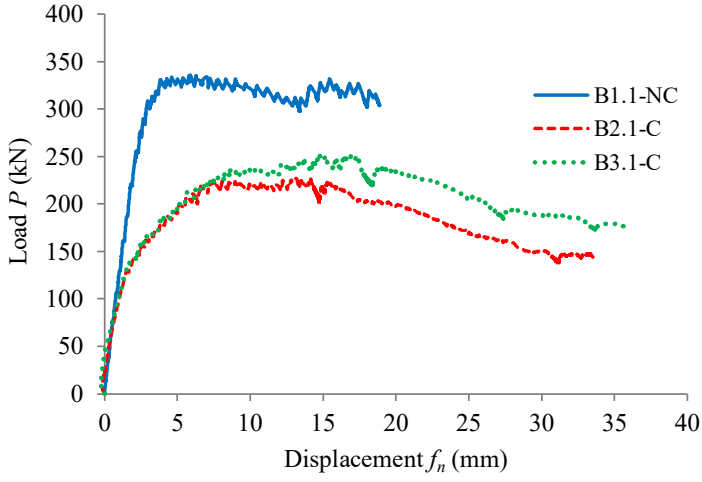

Figure 16. Comparison of load-displacement curves between tested beams

In addition, recent research conducted by Taqi et al. [24] used a similar methodology as the experiment of SFRC beams in this study. A corroded beam with a 0.8% steel fiber volume fraction, the dimensions of $100 \times 150 \times 1300$ mm, and a 2.8 a/d ratio was tested. They reported that the maximum load reached 65.6 kN. In spite of the same concrete properties, the maximum load of SFRC beams in this study has a higher value at around 240 kN. Besides, the reference beam with a 7% corrosion

degree failed due to shear and splitting effects, while the beam specimens in this study still failed by shear-tension mode with a softening behavior.

Table 5. Experimental results of four-point loading test

Beam	Maximum load (kN)	Ratio $P^{C}_{\max}/P^{NC}_{\max}$	Corresponding displacement (mm)	Ratio f^{C}_{n}/f^{NC}_{n}	Failure mode
B1.1-NC	335.87	1.00	5.88	1.00	Flexural-shear
B2.1-C	226.58	0.67	13.18	2.24	Shear-tension with web-shear crack
B3.1-C	251.90	0.75	14.75	2.51	Shear-tension with corroded rebar rupture

4. Conclusions

This paper presents the results obtained on the SFRC beam specimens with the dimensions of $150 \times 200 \times 1100$ mm have a shear span-to-effective depth of 1.5 about the shear strength. Based on the experimental results, the effect of steel corrosion on the shear behavior has been assessed, and the main conclusions can be drawn as follows:

The shear capacity of the non-corroded SFRC beam is improved as evidenced by two features: (i) the shear crack width could be opened to 0.8 mm without brittle collapse; (ii) ductility capacity after post-peak is maintained, corresponding to the development of vertical displacement until 1/50 of the beam span, even with crushing concrete in the compression zone.

Meanwhile, with 16.4% and 24.1% average degrees of corrosion for tensile longitudinal reinforcement and stirrups, the maximum shear strength of corroded SFRC beams is reduced by 25% to 33% compared to that of the non-corroded beam. On the other hand, the residual shear strength of these corroded beams is close to 43–52% of the maximum load of the non-corroded beam.

Under the effect of reinforcement corrosion, the failure mode of SFRC beams can be shifted from flexural-shear to shear-tension, with the significant values of shear crack width and vertical displacement and potential of the corroded rebar rupture.

Acknowledgments

This research is supported by Hanoi University of Civil Engineering (HUCE) under grant number 25-2022/KHXD. The authors would like to thank the Laboratory of Construction Testing and Inspection in HUCE for supporting the experimental works.

References

[1] ACI 544.1 R-96 (2009). *State-of-the-art report on fiber reinforced concrete*. American Concrete Institute, Farmington Hills, MI, USA.

[2] Lim, W.-Y., Hong, S.-G. (2016). Shear tests for ultra-high performance fiber reinforced concrete (UHPFRC) beams with shear reinforcement. *International Journal of Concrete Structures and Materials*, 10 (2):177–188.

[3] Nguyen, N. T., Bui, T.-T., Bui, Q.-B. (2022). Fiber reinforced concrete for slabs without steel rebar reinforcement: Assessing the feasibility for 3D-printed individual houses. *Case Studies in Construction Materials*, 16:e00950.

[4] Bui, T. T., Nana, W. S. A., Doucet-Ferru, B., Bennani, A., Lequay, H., Limam, A. (2020). Shear performance of steel fiber reinforced concrete beams without stirrups: experimental investigation. *International Journal of Civil Engineering*, 18(8):865–881.

[5] Biolzi, L., Cattaneo, S., Mola, F. (2014). Bending-shear response of self-consolidating and high-performance reinforced concrete beams. *Engineering Structures*, 59:399–410.

[6] ACI 318-19 (2019). *Building code requirements for structural concrete and commentary*. American Concrete Institute, Farmington Hills, MI, USA.

[7] Soltani, M., Safiey, A., Brennan, A. (2019). A state-of-the-art review of bending and shear behaviors of corrosion-damaged reinforced concrete beams. *ACI Structural Journal*, 116(3).

[8] Tan, N. N., Nguyen, N. D. (2019). An experimental study on flexural behavior of corroded reinforced concrete beams using electrochemical accelerated corrosion method. *Journal of Science and Technology in Civil Engineering (STCE) - NUCE*, 13(1):1–11.

[9] Nguyen, N. D., Tan, N. N. (2019). Prediction of residual carrying capacity of RC column subjected inplane axial load considering corroded longitudinal steel bars. *Journal of Science and Technology in Civil Engineering (STCE) - HUCE*, 13(2V):53–62. (in Vietnamese).

[10] Rodriguez, J., Ortega, L., Casal, J. (1997). Load carrying capacity of concrete structures with corroded reinforcement. *Construction and Building Materials*, 11(4):239–248.

[11] Zhu, W., François, R., Fang, Q., Zhang, D. (2016). Influence of long-term chloride diffusion in concrete and the resulting corrosion of reinforcement on the serviceability of RC beams. *Cement and Concrete Composites*, 71:144–152.

[12] Zhu, W., François, R., Coronelli, D., Cleland, D. (2013). Effect of corrosion of reinforcement on the mechanical behaviour of highly corroded RC beams. *Engineering Structures*, 56:544–554.

[13] Tan, N. N., Kien, N. T. (2021). An experimental study on the shear capacity of corroded reinforced concrete beams without shear reinforcement. *Journal of Science and Technology in Civil Engineering (STCE) - NUCE*, 15(1):55–66.

[14] Tan, N. N., Kien, N. T. (2020). Modeling the flexural behavior of corroded reinforced concrete beams with considering stirrups corrosion. *Journal of Science and Technology in Civil Engineering (STCE) - NUCE*, 14(3):26–39.

[15] Nguyen, T. K., Nguyen, N. T. (2021). Finite element investigation of the shear performance of corroded RC deep beams without shear reinforcement. *Case Studies in Construction Materials*, 15:e00757.

[16] Li, J., Wu, C., Liu, Z.-X. (2018). Comparative evaluation of steel wire mesh, steel fibre and high performance polyethylene fibre reinforced concrete slabs in blast tests. *Thin-Walled Structures*, 126:117–126.

[17] Lee, J.-H., Cho, B., Choi, E. (2017). Flexural capacity of fiber reinforced concrete with a consideration of concrete strength and fiber content. *Construction and Building Materials*, 138:222–231.

[18] Chalioris, C. E., Sfiri, E. F. (2011). Shear performance of steel fibrous concrete beams. *Procedia Engineering*, 14:2064–2068.

[19] Kwak, Y. K., Eberhard, M. O., Kim, W. S., Kim, J. (2002). Shear strength of steel fiber-reinforced concrete beams without stirrups. *ACI Structural Journal*, 99(4):530–538.

[20] Amin, A., Foster, S. J. (2016). Shear strength of steel fibre reinforced concrete beams with stirrups. *Engineering Structures*, 111:323–332.

[21] Biolzi, L., Cattaneo, S. (2017). Response of steel fiber reinforced high strength concrete beams: Experiments and code predictions. *Cement and Concrete Composites*, 77:1–13.

[22] Berrocal, C. G., Lundgren, K., Löfgren, I. (2013). Influence of steel fibres on corrosion of reinforcement in concrete in chloride environments: A review. In *7th International Conference Fibre Concrete 2013 Proceedings*.

[23] Anandan, S., Manoharan, S. V., Sengottian, T. (2014). Corrosion effects on the strength properties of steel fibre reinforced concrete containing slag and corrosion inhibitor. *International Journal of Corrosion*, 2014:1–7.

[24] Taqi, F. Y., Mashrei, M. A., Oleiwi, H. M. (2021). Experimental study on the effect of corrosion on shear strength of fibre-reinforced concrete beams. *Structures*, 33:2317–2333.

[25] EN 1992-1-1 (2004). *Design of concrete structures - Part 1-1: General rules and rules for buildings*. European Committee for Standardization, Brussels, Belgium.

[26] TCVN 9346:2012. *Concrete and reinforced concrete structures - Requirements of protection from corrosion in marine environment*.

[27] Tan, N. N., Hiep, D. V. (2020). Empirical models of corrosion rate prediction of steel in reinforced concrete structures. *Journal of Science and Technology in Civil Engineering (STCE) - NUCE*, 14(2): 98–107.

[28] François, R., Laurens, S., Deby, F. (2018). *Corrosion and its consequences for reinforced concrete structures*. Elsevier.

[29] ASTM G1-03 (2003). *Standard practice for preparing, cleaning, and evaluating corrosion test*. American Society for Testing and Materials, West Conshohocken, PA.